Dynamical Jahn-Teller effect in polymorphs: Model for the optical vibronic states of Mn^{2+} in polymorphic ZnS

R. Parrot,* A. Geoffroy, and C. Naud
Université Pierre et Marie Curie, Laboratoire de Luminescence,† Tour 13,4, Place Jussieu, 75230 Paris Cedex 05, France

W. Busse and H. E. Gumlich
Technische Universität Berlin, Institut für Festkörperphysik, Jebensstrasse 1, 1000 Berlin 12, Germany

(Received 20 May 1980)

The structures of the ^4E, $^4T_2$, and $^4T_1$ states of Mn^{++} in the axial centers of ZnS polytypes are compared to the structures observed in cubic sites, and a unified model for all vibronic states considered is elaborated which provides a coherent description of a complex spectral distribution in a polymorph. First, from a detailed analysis of recent experimental results obtained from site selection spectroscopy and uniaxial stress experiments, it is shown that the structures of the ^4E states are identical for the cubic and axial sites and that all the observed structures for the orbital triplet states associated with the cubic and axial sites can be analyzed in terms of a Jahn-Teller coupling to degenerate or almost degenerate E vibrational modes. The strength of the Jahn-Teller coupling and the Jahn-Teller shift with respect to the electronic states is determined for each level of Mn^{++} in the cubic and axial centers. Then, the shifts of the electronic states ^4E, $^4T_2$, and ^4E for Mn^{++} in axial symmetry with respect to the electronic states in cubic symmetry are analyzed in terms of totally symmetric electronic interactions with local strains and with the ligand field of distant neighbors. The ^4E states of a d^5 configuration being most likely sensitive to the ligand field of the first neighbors only, the shifts of the ^4E electronic states for the axial centers are interpreted in terms of local strains of A_1 symmetry acting on the MnS_4 clusters. By interpreting the stress-induced shifts of the ^4E states and the shifts in axial centers in a molecular cluster model it is shown that the local A_1 strains most likely correspond to dilatations of the MnS_4 clusters for axial centers. Finally, the shifts of the $^4T_2$ and $^4T_1$ electronic states are interpreted in part in terms of the local A_1 strains and in part in terms of the variation of the ligand field of A_1 symmetry in stacking faults. The energy levels of the Mn^{++} in wurtzite are also tentatively analyzed in the framework of the proposed model.

I. INTRODUCTION

The elaboration of phenomenological models and theoretical grounds for explaining the vibronic properties of a variety of impurities in solids has attracted a continuous interest since the pioneering works in this subject.[1] For example, very intricate experiments and interpretations permitted establishing a vibronic model for the F center in CaO,[2] a model for the Jahn-Teller (JT) coupling between electronic states E and T_2 of a given configuration[3] or different configurations in the case of the F center,[4] and tests of validity of the vibronic and cluster models for an E state.[5] In this paper we report the first attempt to include the Jahn-Teller effect in the interpretation of the spectral distribution of d ions in polymorphs.

One of the most studied polymorphs in relation to the Jahn-Teller effect is probably ZnS which can be grown with the zinc-blende structure (site symmetry T_d), the wurtzite structure (site symmetry C_{3v}) and with the zinc-blende structures with stacking faults[6] (SF); in this case cubic sites of T_d symmetry and several inequivalent sites of C_{3v} symmetry appear as a consequence of irregular sequences of close-packed ZnS layers along a common $[111]_W$ axis of the cubic parts. At this time, detailed descriptions of the vibronic interactions for various levels of d ions as Fe^{++},[7] Ni^{++},[8] Co^{++},[9] Cu^{++},[10] Cr^{++},[11] and Mn^{++},[12–15] are available only for the cubic sites of ZnS. As for the very puzzling spectral distributions in SF's and wurtzite, an inconclusive model where the vibronic interactions are neglected has been reported for several states of Mn^{++}.[16] We will show herein that the Jahn-Teller effect is of primary importance to analyze the relatively large shifts of the centers of gravity of the $^4T_1$, $^4T_2$, and E levels of Mn^{++} in axial sites with respect to the levels in cubic sites and to explain all observed fine-structure patterns.

For each state ^4E, $^4T_2$, and $^4T_1$, the Jahn-Teller effect will be analyzed as follows. First, the symmetry of the effective phonon to which the state is coupled is deduced from uniaxial stress experiments. It will be shown that all studied states of Mn^{++} in cubic and axial sites are coupled to two-dimensional E modes. Second, for each state, the Jahn-Teller effect is described in terms of the Jahn-Teller energy E_{JT} and in terms of the energy $\hbar\omega_E$ of the effective phonon. The energy of the effective phonon could be considered as a fitting parameter, however in most cases, the limitations for $\hbar\omega$ imposed by the phonon spectra and the phonon density of states are so drastic that only one or two values for $\hbar\omega$ can be considered. In our case, it will be shown in the following that the energy of the effective mode of ZnS is $\hbar\omega E = 100$ cm^{-1} for all studied states of Mn^{++}. The Jahn-Teller energy is considered as a fitting parameter varying in relatively large limits since only a very crude value of E_{JT} can be obtained from Ham's cluster model[7] when the orbit-lattice coupling constants are known from uniaxial stress effects and when the energy of the effective phonon is known. In the following, the Jahn-Teller energy for the $^4T_1$ and $^4T_2$ states associated with the axial centers will be obtained from a fitting of both the relative positions of the lines appearing in each fine-structure pattern and the relative dipole strengths of the lines.

In Sec. II we briefly recall the structure of the electronic states ^4E, $^4T_1$, and $^4T_2$ of a d^5 ion and summarize the vibronic properties of these states in the case of Mn^{++} in the cubic sites of ZnS.

Site selection spectroscopy with a dye laser recently permitted us to determine unambiguously the energy levels of the ^4E, $^4T_1$, and $^4T_2$ states at lower energy of Mn^{++} in the cubic centers and two prominent axial sites of ZnS as well as the lifetimes of the $^4T_1 \rightarrow {}^6A_1$ transitions associated with these centers.[17] The experimental results relevant to the present study and new experimental results concerning the energy levels of Mn^{++} in stacking faults are reported in Sec. III.

Section IV is devoted to the presentation of a model Hamiltonian which permits analyzing first the vibronic interactions governing the structure of the fundamental vibronic lines (FVL) of the orbital doublet and triplet states of Mn^{++} in cubic and axial sites and second the vibronic shifts and the totally symmetric electronic interactions contributing to the shifts of the fine-structure lines in axial sites with respect to the fine-structure lines in cubic sites.

A detailed quantitative analysis of the vibronic and electronic interactions in the axial sites is proposed in Secs. V and VI. The analysis of vibronic interactions is mainly deduced from the observed fine-structure pattern and from the uniaxial stress effects on the orbital doublet and triplet states of Mn^{++} in axial and cubic sites. The electronic interactions which shift the axial lines are associated not only with the variations of the cubic part of the ligand field acting on the Mn^{++} centers but also with dilatations of the MnS_4 clusters.

II. ELECTRONIC AND VIBRONIC STRUCTURES OF THE ^4E, $^4T_1$, AND $^4T_2$ STATES OF Mn^{++} IN THE CUBIC SITES OF ZnS

Since the knowledge of the fine structure of the ^4E, $^4T_1$, and $^4T_2$ states of Mn^{++} in cubic sites of ZnS is of primary importance to understand the structure of these states in axial symmetry, we will briefly summarize the most important features of the fine-structure levels associated to the cubic sites (see Fig. 1). The details of the uniaxial stress experiments used to identify the FVL's of each state as well as the analyses which permitted elaborating the Jahn-Teller models are given in previous papers.

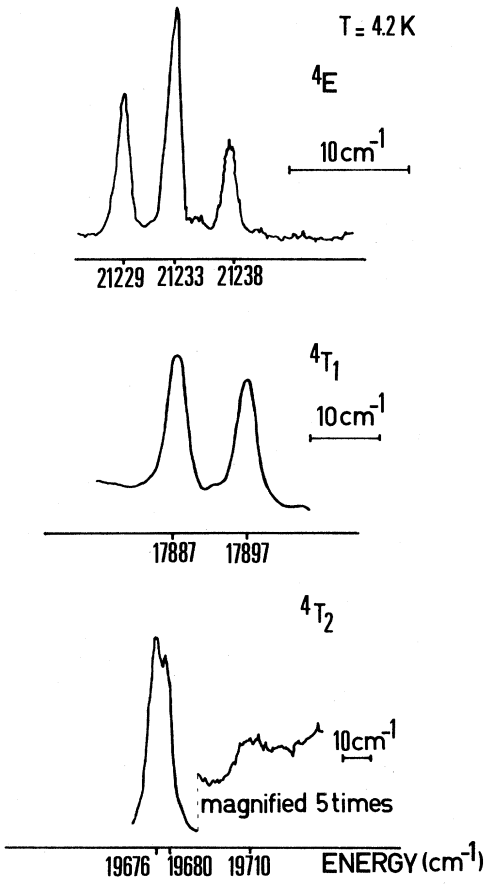

FIG. 1. Fine structure of the ^4E, $^4T_1$, and $^4T_2$ states of Mn^{++} in cubic sites of ZnS.

A. ^4E state

In T_d^* the ^4E states of a d^5 configuration are decomposed into three states Γ_7, Γ_8, and Γ_6, the main contributions to the splitting being due to the spin-spin interaction and the second-order spin-orbit interaction. The three fine-structure lines corresponding to transitions from the almost degenerate $^6A_1$ fundamental state to the ^4E states are equally spaced as it can be shown from symmetry considerations when the spin-spin interaction and the second-order spin-orbit interactions are taken into account. The relative dipole strengths (RDS) are

$$\mathcal{S}[^6A_1 \rightarrow \Gamma_7(^4E)] = 3 \ , \quad \mathcal{S}[^6A_1 \rightarrow \Gamma_8(^4E)] = 5 \ ,$$

and

$$\mathcal{S}[^6A_1 \rightarrow \Gamma_6(^4E)] = 2 \ .$$

In the case of Mn^{++} this structure for a ^4E state (see Fig. 1) has been confirmed by uniaxial stress experiments performed on ZnS (Ref. 15) and also by the fine structures observed in distorted tetrahedral MnX_4 clusters as $MnCl_4$, $MnBr_4$, and $MnSe_4$,[14] in all cases a large splitting of the Γ_8 state has been observed as well as shifts of the Kramers doublets Γ_6 and Γ_7. It has been recently shown that the fundamental vibronic states of the ^4E states of Mn^{++} are predominantly coupled to intrinsic or stress-induced strains of E symmetry, the coupling to T_2 strains being small or negligible.[14] Furthermore, a study of the Jahn-Teller coupling from Ham's cluster model,[18] using the orbit-lattice coupling coefficients of Mn^{++} in ZnS, has shown that the ^4E states are only moderately coupled to E vibrational modes; in the case of Mn^{++} in the cubic sites of ZnS the Huang-Rhys factor was found to be $S = 0.4$, the corresponding reduction factors being $p = 0.35$ for electronic operators of symmetry A_2 and $q = 0.7$ for operators of symmetry E. Approximate expressions for p and q are given by Ham[18]

$$p = \exp(-1.974 S^{0.761}) \ ,$$

where $S = E_{JT}/\hbar\omega$ and $q = \frac{1}{2}(1+p)$. The energy $\hbar\omega$ of the effective phonon was chosen to be 100 cm^{-1} and therefore[19] the Jahn-Teller energy is 40 cm^{-1}.

B. $^4T_1$ state

In T_d^* a $^4T_1$ state is decomposed into two Kramers doublets Γ_6 and Γ_7 and two Γ_8 states. In the absence of a Jahn-Teller coupling, the splittings arise mainly from the first-order spin-orbit interaction and to a lesser extent from a second-order spin-orbit interaction. The RDS's of the $^6A_1 \rightarrow {}^4T_1$ transitions for a d^5 ion are given by symmetry considerations; they are

$$\mathcal{S}[^6A_1 \rightarrow \Gamma_6(^4T_1)] = 45 \ , \quad \mathcal{S}[^6A_1 \rightarrow \Gamma_7(^4T_1)] = 20 \ ,$$

$$\mathcal{S}[^6A_1 \rightarrow \Gamma_8(\tfrac{3}{2})(^4T_1)] = 63 \ ,$$

and

$$\mathcal{S}[^6A_1 \rightarrow \Gamma_8(\tfrac{5}{2})(^4T_1)] = 22 \ ,$$

for dipolar electric transitions. In the case of the fluorescent $^4T_1$ state of Mn^{++} in the cubic sites of ZnS (see Fig. 1) it has been demonstrated that the two FVL's which appear in the optical spectra can be interpreted in terms of a relatively strong coupling to E vibrational modes.[12] *The observed lines correspond to the transitions:*

$$|^6A_1\rangle \rightarrow |\Gamma_7\rangle, \frac{3}{\sqrt{10}}|\Gamma_8(\tfrac{3}{2})\rangle - \frac{1}{\sqrt{10}}|\Gamma_8(\tfrac{5}{2})\rangle$$

for the line at lower energy, the RDS being 33, and to the transition

$$|^6A_1\rangle \rightarrow |\Gamma_6\rangle, \frac{1}{\sqrt{10}}|\Gamma_8(\tfrac{3}{2})\rangle + \frac{3}{\sqrt{10}}|\Gamma_8(\tfrac{5}{2})\rangle$$

for the line at higher energy, the RDS being 27. The Huang-Rhys parameter is $S = 1.9$, the energy of the effective phonon of E symmetry being 100 cm^{-1}.[12]

C. $^4T_2$ state

An electronic $^4T_2$ state decomposes into a Γ_6, a Γ_7, and two Γ_8 states in T_d^*. For a d^5 ion the RDS's of the $^6A_1 \rightarrow {}^4T_2$ transitions are

$$\mathcal{S}[^6A_1 \rightarrow \Gamma_6(^4T_2)] = 7 \ , \quad \mathcal{S}[^6A_1 \rightarrow \Gamma_7(^4T_2)] = 0 \ ,$$

$$\mathcal{S}[^6A_1 \rightarrow \Gamma_8(\tfrac{3}{2})(^4T_2)] = 9 \ ,$$

and

$$\mathcal{S}[^6A_1 \rightarrow \Gamma_8(\tfrac{5}{2})(^4T_2)] = 14 \ ,$$

for electric dipolar transitions. The vibronic structure of the $^4T_2$ state at lower energy of Mn^{++} in the cubic sites of ZnS was among the most complex encountered in Jahn-Teller systems. As shown in Ref. 13 the vibronic states are moderately coupled to E strains ($S = 0.6$) and the overall spin-orbit splitting (110 cm^{-1}), the energy of the effective phonon[19] (100 cm^{-1}) and the vibronic shifts (60 cm^{-1}) have roughly the same magnitude so that a diagonalization of the vibronic and electronic Hamiltonians is needed in order to get a correct description of the vibronic levels and of the relative dipole strengths. Furthermore, a pronounced intensity transfer for the $\Gamma_8(\frac{3}{2})$ state to excited vibronic states seriously complicates the interpretation of experimental results. In that case, symmetry considerations are no longer sufficient to accurately describe the RDS, in fact it is necessary to determine the vibronic wave functions associated with the fundamental vibronic states. This was done by taking into account five phonons. The results of the calculations are summarized in Fig. 1 for the cubic sites. The two lines at lower energy

correspond to the transitions ${}^6A_1 \rightarrow \Gamma_8(\frac{5}{2})$ and ${}^6A_1 \rightarrow \Gamma_6$, the line at higher energy corresponds to the transition ${}^6A_1 \rightarrow \Gamma_8(\frac{3}{2})$ whose intensity is reduced by a selective intensity transfer.

III. EXPERIMENTS

A. Samples and apparatus

The experiments were performed on ZnS:Mn crystals grown by Eagle-Picher. The crystals are identical to those used in previous studies concerning the fine-structure lines of the ${}^4E$ (Refs. 14 and 15), ${}^4T_2$ (Ref. 13), and ${}^4T_1$ (Ref. 12) states. In particular the relative number of Mn^{++} ions in the various axial sites and in the cubic sites is the same for the crystals studied here as for the crystals previously studied. The concentration is approximately 10^{-4} g Mn/g ZnS; this concentration is low enough to prevent the appearance of pair lines in the excitation and absorption spectra.[20]

The emission and excitation spectra were obtained with a dye laser pumped with a molectron nitrogen laser. The peak power was 10^5 W, the pulse time being 10 ns. The decay of the luminescence was recorded with a grating spectrometer associated with a photocounter and an averaging system.

The experiments were performed at 4.2 K in excitation and 4.2 and 15 K in emission.

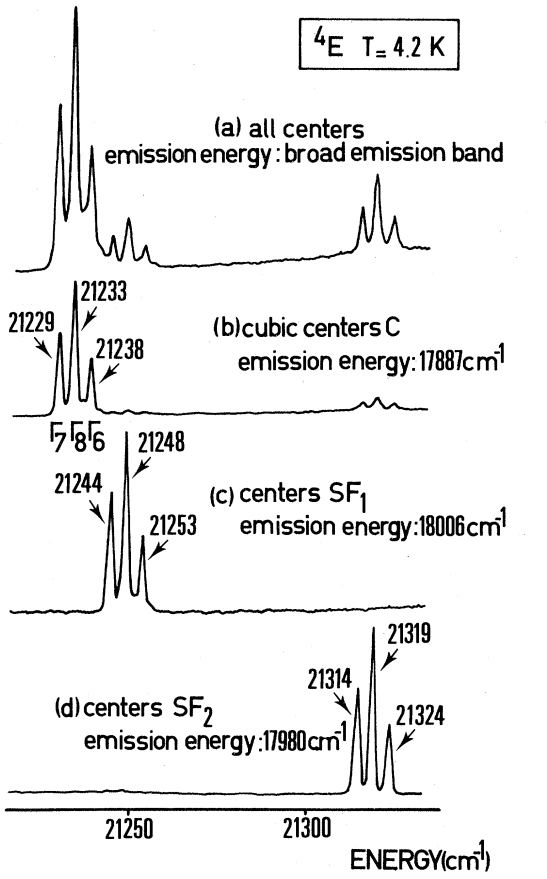

FIG. 2. Excitation spectrum of the ${}^4E$ zero-phonon lines of the ${}^4E$ levels of Mn^{++} in cubic and axial sites of ZnS. (a) Spectrum obtained by recording the emission of the ${}^4T_1$ band. (b) Spectrum obtained by recording the emission at 17 887 cm^{-1} (see Fig. 3); the weak excitation lines appearing near 21 248 and 21 319 cm^{-1} are most likely due to weak excitations of the axial centers, the light emitted at 17 887 cm^{-1} being due to phonon assisted transitions (note the overlap of the zero-phonon lines of the cubic centers in Fig. 3 with the emission bands of the centers SF_1 and SF_2). (c) Spectrum obtained by recording the emission at 18 006 cm^{-1}; no excitation of the centers c and SF_2 is observed in this case since there is no overlap between the zero-phonon lines at 18 006 cm^{-1} and the phonon-assisted lines of the centers c and SF_2 (see Fig. 3). (d) Spectrum obtained by recording the emission at 17 980 cm^{-1}.

B. Experiments

The excitation spectra were obtained by collecting the light emitted by the fundamental vibronic lines (FVL) of Mn^{++} in a given site; conversely the emission spectra were obtained by exciting the FVL's of Mn^{++} in a given site. Parts of the associated emission and excitation spectra are given in Figs. 2–4 for the cubic centers and two prominent axial centers denoted SF_1 and SF_2 (see also Tables I–III). Excitation transfer between different Mn^{++} centers was found to be negligible for the chosen concentration (see Fig. 2), so that no ambiguity remains in associating the emission and excitation spectra of Mn^{++} in SF_1 and SF_2. It can be noted that these experimental results are not in agreement with the associations of FVL's for each site as predicted by a previous electronic model based on the interpretation of optically detected EPR spectra.[16]

Very detailed experiments performed on the ${}^4E$ and ${}^4T_1$ states of the cubic centers and the centers SF_1 and SF_2 have shown the presence of two supplementary Mn^{++} centers. The spectra corresponding to these new centers are partially hidden by the spectra of the centers c, SF_1, and SF_2 (see Figs. 5 and 6), however the existence of these new centers was clearly demonstrated by carefully scanning the emission lines at 17 887 and 17 980 cm^{-1}. These centers show a structure analogous to that of the cubic and axial centers SF_2 (see Tables I and III).

It can be noted (see Figs. 5 and 6) that the spacings between two adjacent FVL's for the ${}^4E$ states are not

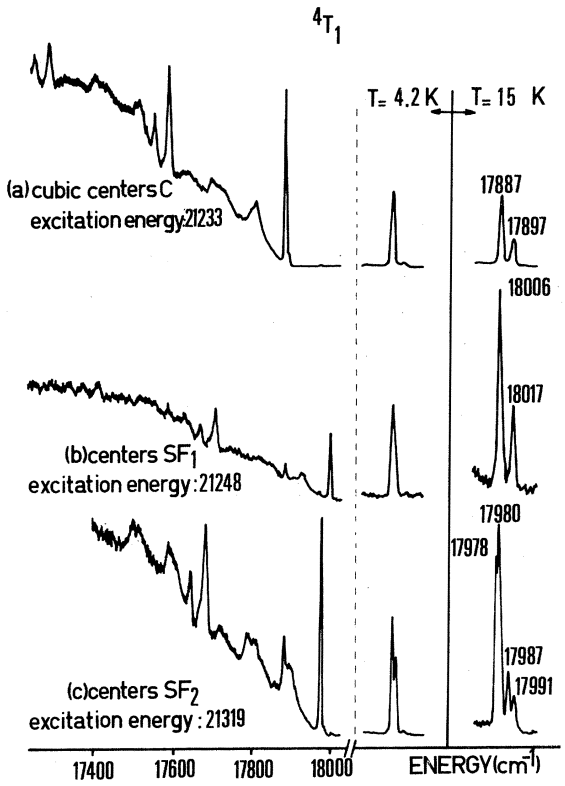

FIG. 3. Emission spectra of the $^4T_1$ states. The details of the zero-phonon lines at 4.2 and 15 K are given in the inserts.

TABLE I. ^4E states. Energies of the fundamental vibronic lines (FVL), positions of the centers of gravity of the fine-structure lines (CG), and calculated dilatations (D) of the MnS_4 clusters with respect to the cubic centers for the centers SF_1, SF_2, and w described in Sec. III.

^4E	Energy of the FVL	Nature of the FVL	CG (cm^{-1})	D
cubic	21 229	Γ_7		
centers	21 233	Γ_8	0	0
c	21 238	Γ_6		
stacking	21 244	Γ_7		
fault	21 248	Γ_8	+15.1	11×10^{-4}
SF_1	21 253	Γ_6		
	21 314	Γ_7		
SF_2	21 319	Γ_8	+85.6	64×10^{-4}
	21 324	Γ_6		
	21 231	Γ_7		
SF_3	21 235	Γ_8	+2.3	2×10^{-4}
	21 240	Γ_6		
	21 316	Γ_7		
SF_4	21 320	Γ_8	+86.9	65×10^{-4}
	21 325	Γ_6		
wurtzite[a]	~21 336		~+103	77×10^{-4}
w				

[a]From Ref. 16.

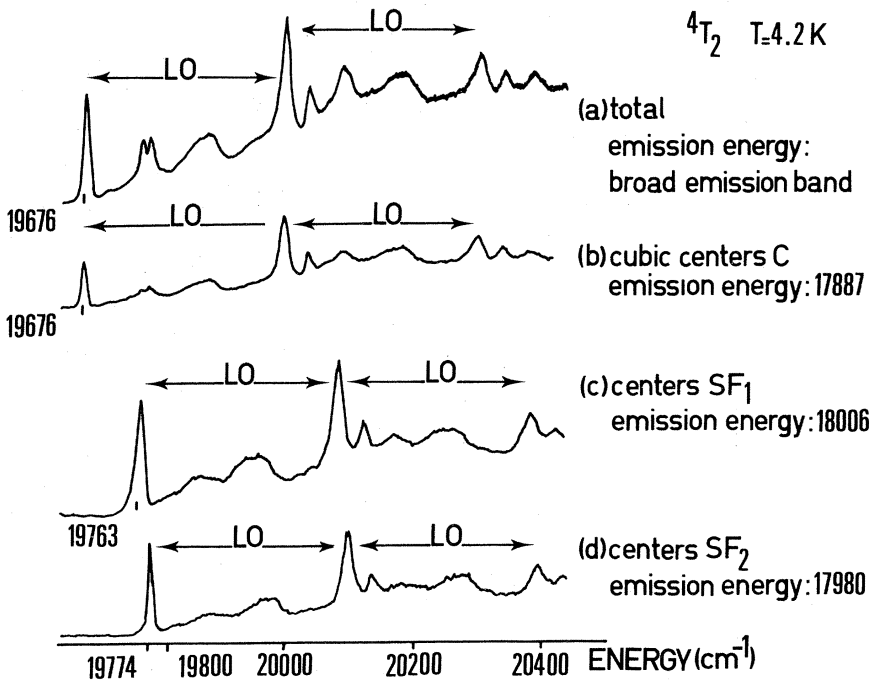

FIG. 4. Overall view of the excitation spectra of the $^4T_2$ band.

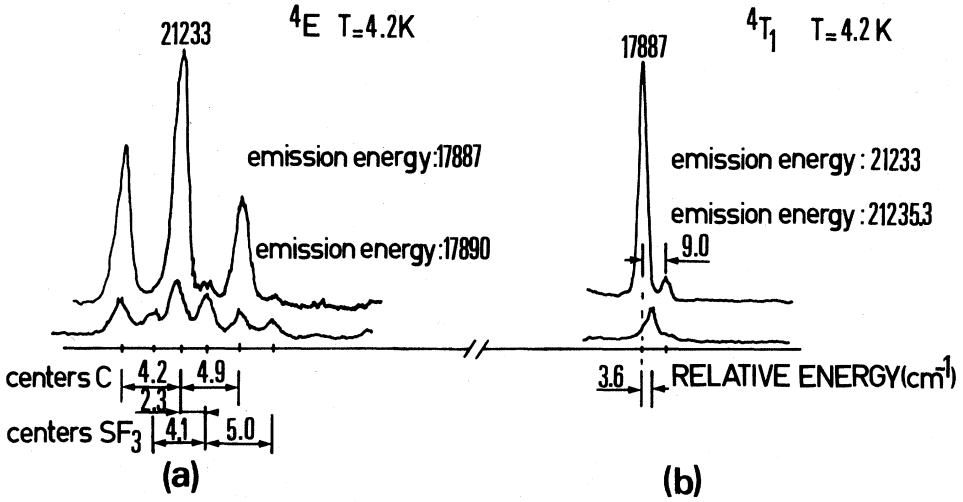

FIG. 5. Excitation spectrum of the ^4E zero-phonon lines (a) and the $^4T_1$ emission (b) of a new nearly cubic center (SF_3). With respect to the cubic lines, the shift of the zero-phonon lines of the ^4E state is of 2.3 cm^{-1}, the shift of the $^4T_1$ emission lines is 3.6 cm^{-1}.

strictly identical as predicted by a model involving the spin-spin interaction and a second-order spin-orbit interaction. Probably higher-order perturbation schemes would be necessary to interpret the slight difference between the observed spacings.

Further experiments were performed on the $^4T_2$ states in order to clearly show the presence of the $\Gamma_8(\frac{3}{2})$ level for the cubic centers and the centers SF_1 and SF_2. Figure 7 shows that, as for the cubic sites, the transitions $^6A_1 \rightarrow \Gamma_8(\frac{3}{2})(^4T_2)$ are subjected to a strong-intensity transfer.

It will now be shown how these definite experimental results used in conjunction with uniaxial stress experiments permit us to elaborate coherent vibronic and electronic models for all centers simultaneously.

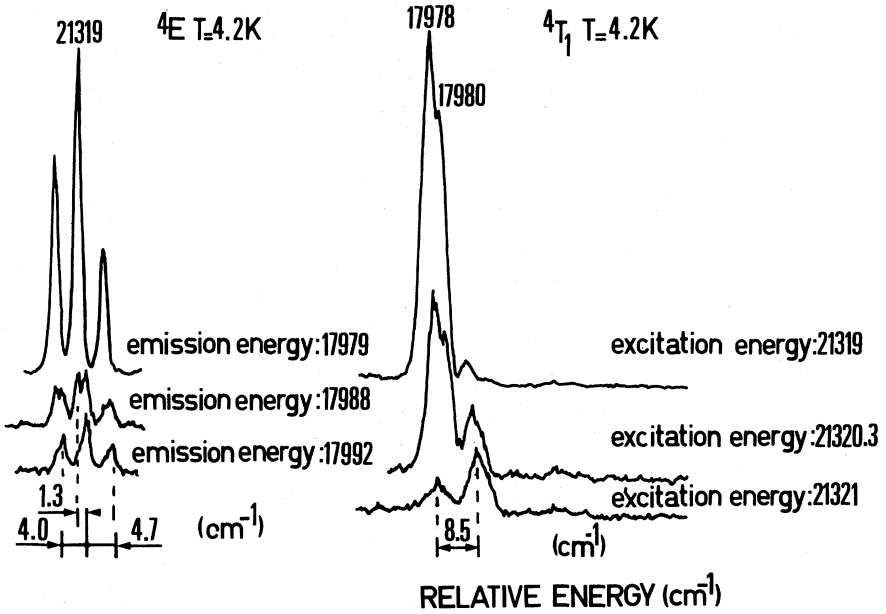

FIG. 6. Excitation and emission spectrum of a new center (SF_4) hidden by the center SF_2. The center of gravity of the ^4E fine structure is shifted by 1.3 cm^{-1} with respect to the center of gravity of the ^4E lines of the center SF_2. The emission is shifted by 8.5 cm^{-1}.

TABLE II. $^4T_2$ states of the centers c, SF_1, SF_2, and w. Energies of the fundamental vibronic lines (FVL), nature of the FVL's. Huang-Rhys factor S, vibronic shifts, and shifts induced by the local strains $\Delta W_{loc}(A_1)$ and the variation of the crystal field $\Delta W_{nc}(A_1)$.

$^4T_2$	Energy of the FVL's (cm^{-1})	Nature of the FVL's[a]	Huang-Rhys factor S	Vibronic shifts ΔW_{vib} (cm^{-1})[b]	$\Delta W_{loc}(A_1)$ (cm^{-1})	$\Delta W_{nc}(A_1)$ (cm^{-1})
c	19676	$\Gamma_8(\frac{5}{2})$				
(cubic	19680	Γ_6	0.6	96	0	0
centers)	19710[c]	$\Gamma_8(\frac{3}{2})$				
SF_1	19763	$\Gamma_8(\frac{5}{2})$				
(stacking	~19763	and Γ_6	0.4	82	+20	+53
fault)	19805[c]	$\Gamma_8(\frac{3}{2})$				
	19774	$\Gamma_8(\frac{5}{2})$				
SF_2	19780	Γ_6	0.5	89	+115	−24
	19811[c]	$\Gamma_8(\frac{3}{2})$				
w (wurtzite)	~19861[d]		~0.6	~96	+138	~47

[a]The transition $^6A_1 \rightarrow \Gamma_7(^4T_2)$ is strictly forbidden in T_d symmetry. The nature of the FVL's is only roughly given by the representations of T_d^* as explained in Sec. II.

[b]These shifts are those of the $\Gamma_8(\frac{5}{2})$ line with respect to the $^4T_2$ electronic states.

[c]Lines subjected to a strong-intensity transfer.

[d]From Ref. 16.

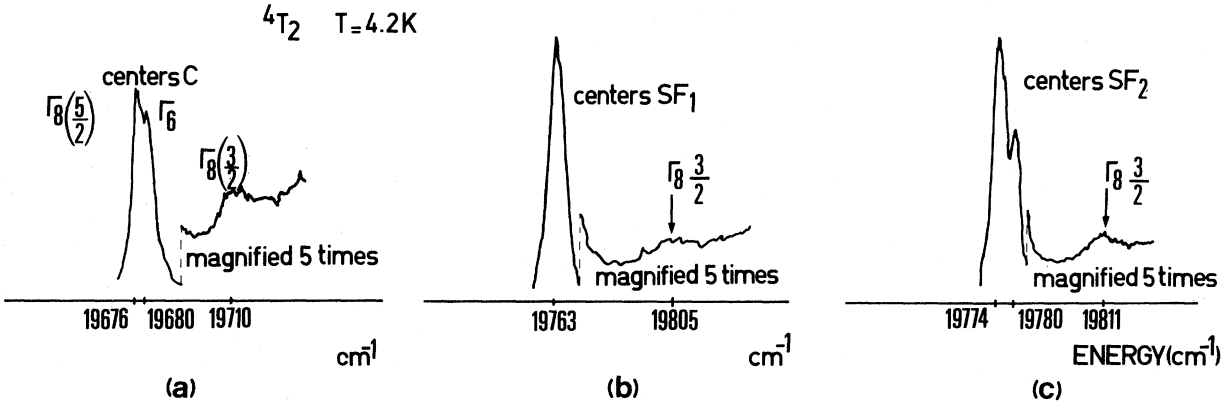

FIG. 7. Details of the fundamental vibronic lines of the $^4T_2$ states for the centers c, SF_1, and SF_2. The line at higher energy corresponds to the transition $^6A_1 \rightarrow \Gamma_8(\frac{3}{2})$ $(^4T_2)$ subjected to a strong-intensity transfer. The transition $^6A_1 \rightarrow \Gamma_7$ is strictly forbidden. These excitation spectra were obtained by recording the emission of the cubic centers at 17887 cm^{-1} (a), the emission of the centers SF_1 at 18006 cm^{-1} (b), and the emission of the centers SF_2 at 17980 cm^{-1}(c).

IV. MODEL HAMILTONIAN

The basic Hamiltonian of the proposed model is

$$\mathcal{H}=\mathcal{H}_c+\mathcal{H}_{SO}+\mathcal{H}_{SS}+\sum_{\Gamma}\Delta\mathcal{H}_c(\Gamma)+\mathcal{H}_{vib}+\text{other terms}\ ,$$

where $\mathcal{H}_c$ is the Hamiltonian governing the multiplets Γ in cubic sites. $\mathcal{H}_{SO}$ and $\mathcal{H}_{SS}$ are, respectively, the spin-orbit and spin-spin Hamiltonians. $\sum_\Gamma \Delta\mathcal{H}_c(\Gamma)$ is a perturbation of $\mathcal{H}_c$, around the d ions in axial centers, expressed in terms of operators spanning the representation Γ of the cubic group.

$\mathcal{H}_{vib}$ is the vibronic Hamiltonian associated with a state $^{2S+1}\Gamma$; the main effect of $\mathcal{H}_{vib}$ on doublet and triplet states is to reduce the fine-structure splittings and to shift the centers of gravity of the FVL's with respect to the electronic states. For our purpose, the "other terms" include primarily the stress-induced Hamiltonian $\mathcal{H}_{stress}$.

In order to describe a Jahn-Teller state in an axial center with respect to the corresponding electronic state Γ in cubic sites, it is convenient to separate the totally symmetric interactions A_1 contributing to the shifts $\Delta W(\Gamma)$ of the gravity centers of the FVL's of the state Γ from the interactions governing the fine-structure pattern. By extracting the preponderant interactions A_1 from $\mathcal{H}$, we get

$$\Delta W(\Gamma)=\Delta W_c+\Delta W_{vib}+\Delta W_{SO}+\Delta W_{stress}\ ,$$

the notations are obvious, except for ΔW_{SO} which represents the variation of the shift due to spin-spin and second-order spin-orbit interactions.

Following this procedure the problems to solve for each Γ state are: (i) determine quantitatively the various terms in $\Delta W(\Gamma)$ for the axial centers independent of crystallographic models and predictions of crystal-field or covalent models (which proved misleading in previous models for Mn^{++} centers) (ii) determine the contribution of non-A_1 interactions to the fine-structure pattern.

It will be shown in Sec. V how this can be achieved in the case of Mn^{++} centers in ZnS from an analysis of the ^4E, $^4T_1$, and $^4T_2$ states considered in that order. However, before considering the details of the proposed model several remarks are to be made.

First, in previous studies on the optical energy levels of d ions in stacking faults, the term $\Delta\mathcal{H}_c(A_1)$ only has been considered for various axial centers in ZnS.[16] Explicitly, the axial crystal field acting on an impurity in a stacking fault is of the form

$$V=\gamma_2^0C_0^2+\gamma_3^0C_0^3+\gamma_3^3C_3^3+\gamma_4^0C_0^4+\gamma_4^3C_3^4$$

{the C^k's are electronic operators related to the classical spherical harmonics by $C^k=[4\pi/(2k+1)]^{1/2}Y^k$}, and the contribution to $\Delta\mathcal{H}_c(A_1)$ is given by

$$[\Delta\mathcal{H}_c(A_1)]_V=\left(\gamma_4^0-\frac{2\sqrt{5}}{\sqrt{7}}\gamma_4^3\right)\Big/\left(1+\tfrac{20}{7}\right)\left(C_0^k-\frac{2\sqrt{5}}{\sqrt{7}}C_3^4\right)$$

$$+\left(\gamma_3^0-\frac{2}{\sqrt{5}}\gamma_3^3\right)\Big/\left(1+\tfrac{4}{5}\right)\left(C_0^3-\frac{2}{\sqrt{5}}C_3^3\right)\ .$$

The variation of the cubic field parameter Dq which depends on the electronic operators C_4 had been calculated in a point-charge model by using the bond lengths and angles as given by the crystallographic data and the results of this calculation have been used as a guide to determine the energy levels associated to the axial centers.[16] However, it must be recalled that this kind of calculation is of little help to explain the strength of the coupling of the electronic states of Mn^{++} to A_1, E, and T_2 intrinsic or stress-induced strains.[12–14] Therefore it is not surprising that this simple model fails in predicting the energy levels of Mn^{++} in stacking faults.

Second, it must be emphasized that the proposed Hamiltonian contains a vibronic term which allows for different Jahn-Teller shifts for the electronic states of the cubic and axial centers. Therefore, we will first determine the Jahn-Teller shifts for all states considered in order to obtain the electronic shifts and then discuss the origin of these electronic shifts.

V. VIBRONIC AND ELECTRONIC INTERACTIONS IN THE ^4E, $^4T_1$, AND $^4T_2$ STATES OF Mn^{++} IN THE AXIAL CENTERS OF ZnS

A. ^4E state

The fine-structure patterns for the ^4E states in cubic and axial sites are identical. In particular, (i) there is no observable splitting of the central Γ_8 line in axial centers and the energy differences $W(\Gamma_7)-W(\Gamma_8)$ and $W(\Gamma_6)-W(\Gamma_8)$ between two consecutive lines are equal for the cubic and axial centers. The uniaxial stress effects are almost identical for each fine-structure pattern of SF centers.[15] In particular, (ii) the stress-induced splittings of the Γ_8 states and the shifts of the Γ_6 and Γ_7 states are almost identical for $\vec{P}\parallel[1\bar{1}0]$ (see Fig. 8) and all lines are almost unsensitive to an applied pressure parallel to the $[111]_W$ crystallographic axis, and (iii) the linear stress-induced shifts due to $\epsilon(A_1)$ strains are identical for $\vec{P}\parallel[1\bar{1}0]$ and almost identical for $\vec{P}\parallel[111]_W$ (for $P=36\times10^8$ dyn/cm^2, the shifts are -17.1 cm^{-1} for centers c, -15.3 cm^{-1} for centers SF_1 and -14.6 cm^{-1} for centers SF_2).

The experimental results (i) and (ii) show that the

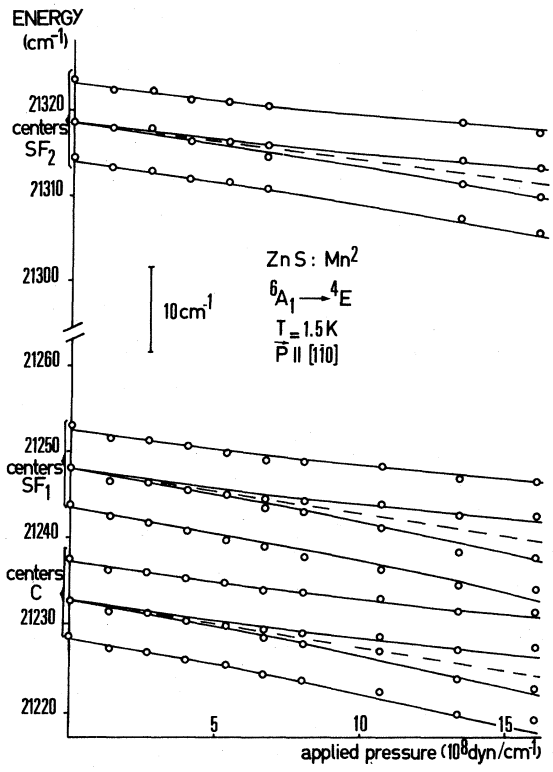

FIG. 8. Uniaxial stress effect on the ^4E state of Mn^{++} in the centers c, SF_1, and SF_2, and energy levels in terms of a linear coupling to intrinsic or stress-induced strains. The dashed lines represent the shifts due to the $\epsilon(A_1)$ strains.

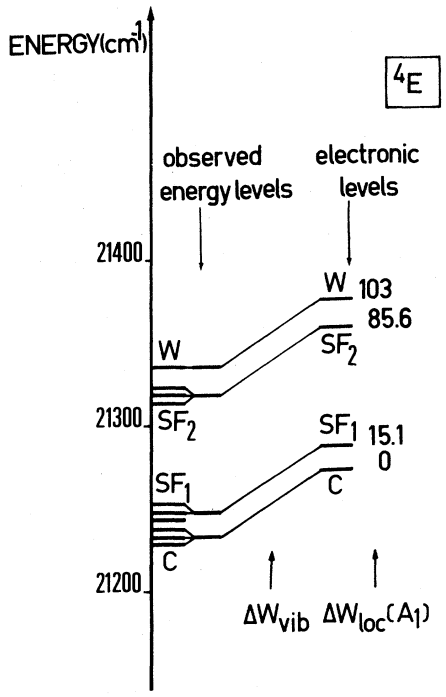

FIG. 9. Model for the totally symmetric and electronic interactions for the ^4E states of the centers c, SF_1, SF_2, and w. ΔW_{vib} represents the Jahn-Teller shift common to all centers. The shifts $\Delta W_{loc}(A_1)$ of the electronic states of the axial centers are given in units of cm^{-1}. As discussed in Secs. V A and VI, these shifts are most likely due to dilatations of the MnS_4 clusters.

Jahn-Teller effect is *almost* identical for the cubic and SF centers and that the ^4E states are coupled to two-dimensional E modes in cubic symmetry or to almost degenerate two-dimensional modes in axial symmetry. Therefore, the fine-structure pattern for the cubic and SF centers are primarily governed by the operator $q(\mathcal{H}_{SO}^2 + \mathcal{H}_{SS})_E$, q being the reduction parameter defined in Sec. III. This reduction parameter is the same for all centers, the index E means that only the part of $\mathcal{H}_{SO}^2$ and $\mathcal{H}_{SS}$ which spans the representation E of T_d is to be considered. The nonreduced electronic shifts ΔW_{SO} due to $(\mathcal{H}_{SO}^2 + \mathcal{H}_{SS})A_1$ will not be explicitly considered as being probably almost identical for all centers. As shown in Sec. III, an evaluation of the Jahn-Teller coupling from Ham's cluster model and from the orbit-lattice coupling coefficient (OLCC) of Mn^{++} in ZnS gives $E_{JT} = 40\ cm^{-1}$ and $q \sim 0.7$. (The energy of the effective phonon being $\hbar\omega_E = 100\ cm^{-1}$.)

From these values we can conclude that the *electronic* ^4E states for all centers are shifted by 40 cm^{-1} with respect to the FVL's (Fig. 9) and that they are only weakly (or not) coupled to the noncubic terms $\Delta\mathcal{H}_c(\Gamma \neq A_1)$ whose influence does not appear on the observed fine-structure pattern in axial sites. The operators $\Delta\mathcal{H}_c(\Gamma = A_2)$ are reduced by a factor $p \sim 0.35$, and the operators $\Delta\mathcal{H}_c(\Gamma)$ which can act on the ^4E states through second-order interaction involving the spin-orbit interaction are reduced by the factor p when $\Gamma = T_2$ and q when $\Gamma = T_1$ with $q = 0.7$.

In order to proceed further with the electronic model for axial centers we have to consider the stress effects (c). First, the shifts of the axial lines with respect to the cubic lines are of the same order of magnitude as the maximum stress-induced linear shifts, which justifies the hypothesis of a linear relationship (LR) between the shifts and the variations $\Delta\mathcal{H}_c(A_1)$ of the internal field. Second, the shifts of the axial lines are towards higher energy while the stress-induced shifts due to A_1 strains are towards lower energy, strongly supporting the hypothesis that the main contribution to $\Delta\mathcal{H}_c(A_1)$ is due to a dilatation of the lattice around the Mn^{++} centers. A quantitative estimate of this dilatation can be obtained from a cluster model restricted to the first neighbors since in this model, the LR hypothesis means that the observed shifts are proportional to the strains $\epsilon(A_1)$ associated to the first neighbors whatever the nature (local or stress-induced) of these strains. From the OLCC's corresponding to A_1 strains, we get

$\Delta W(A_1) = 13\,400$ cm^{-1} per unit A_1 strain and $\epsilon(A_1)_{SF_1} = 11 \times 10^{-4}$, $\epsilon(A_1)_{SF_2} = 64 \times 10^{-4}$ [and $\epsilon(A_1)_w = 77 \times 10^{-4}$ by tentatively assuming that the OLCC's in wurtzite are identical to those in SF's, see Table I]. It must be noted that another description of the dilation of the lattice can be made in terms of the covalency parameter $1-k^2$ intervening in the cluster model for MnS_4 (Ref. 21) by taking $d(1-k^2)/dW(A_1) = -30 \times 10^{-6}$ cm.

B. $^4T_1$ states

As shown in Ref. 12 the two FVL's associated with each c and SF_1 center show identical shifts and splittings under an applied pressure $\vec{P} \parallel [1\bar{1}0]$ and no splitting for $\vec{P} \parallel [111]_W$ (see Fig. 10); this shows that these two centers are coupled only to E stress-induced strains (and A_1 strains). Therefore the observed vibronic structures are interpreted in terms of a strong Jahn-Teller coupling to E modes, the line at lower energy corresponding to the almost degenerate states $|\Gamma_7, 00\rangle$ and $(3/\sqrt{10})|\Gamma_8(\frac{3}{2}), 00\rangle - (1/\sqrt{10})|\Gamma_8(\frac{5}{2}), 00\rangle$ and the other line to the states $|\Gamma_6, 00\rangle$ and $(1/\sqrt{10})|\Gamma_8(\frac{3}{2}), 00\rangle + (3/\sqrt{10})|\Gamma_8(\frac{5}{2}), 00\rangle$. The shifts of the vibronic states with respect to the electronic states for both centers are $\Delta W_{vib} = -190$ cm^{-1} ($S = 1.9$, $\hbar\omega_E = 100$ cm^{-1}). (A vibronic shift of -190 cm^{-1} has also been tentatively taken for the centers w which show the same structure as the centers c for $\vec{P} = 0$.)

For the centers SF_2, the observation of four vibronic lines is a clear indication that they are less coupled to almost degenerate E modes than the centers c and SF_1. From an analysis of the splitting of a $^4T_1$ state in terms of the Huang-Rhys parameter we obtained $S \sim 1.4$ and $\Delta W_{vib} \sim -140$ cm^{-1} (Fig.

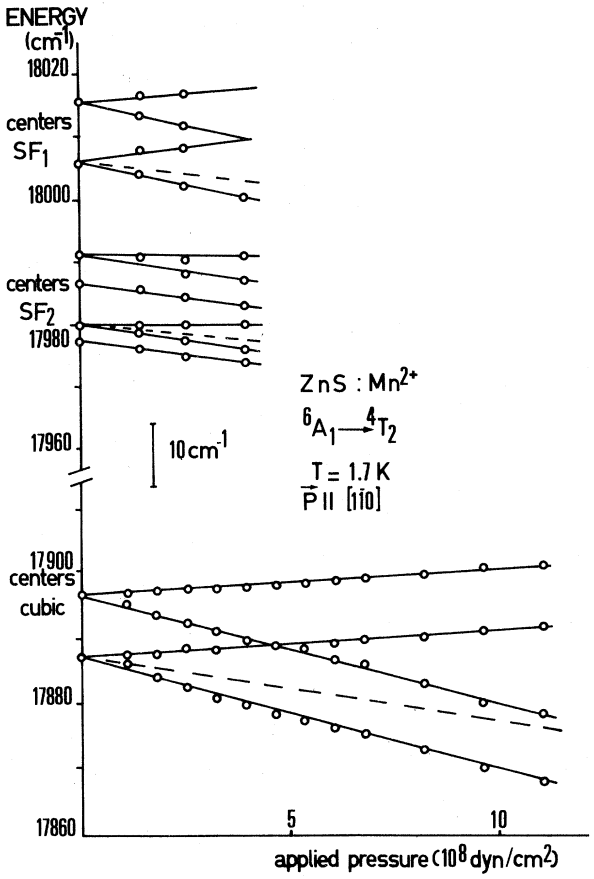

FIG. 10. Uniaxial stress effect on the fundamental vibronic lines of the $^4T_1$ states of Mn^{++} for the centers c, SF_1, and SF_2. The dashed lines represent the shifts due to the $\epsilon(A_1)$ strains.

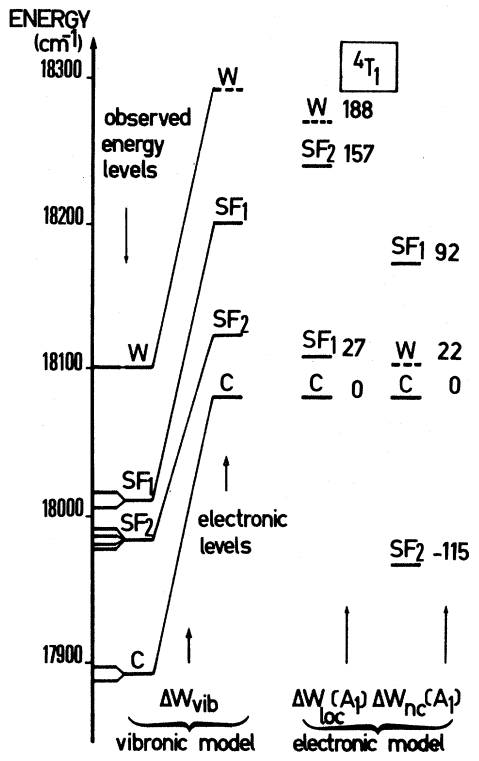

FIG. 11. $^4T_1$ states. Energy-level scheme showing the contribution of the vibronic shifts and electronic interactions to the shifts of the centers SF_1, SF_2, and w. The shifts of the electronic levels of the axial centers are decomposed into shifts $\Delta W_{loc}(A_1)$ due to dilatations of the MnS_4 clusters and shifts $\Delta W_{nc}(A_1)$ whose origin is discussed in Sec. VI. For a given axial center the sum of $\Delta W_{loc}(A_1)$ and $\Delta W_{nc}(A_1)$ gives the position of the electronic level of the axial center with respect to the electronic level of the cubic center. Shifts in cm^{-1}.

11). The fact that the $|\Gamma_8(\frac{3}{2}),00\rangle$ and $|\Gamma_8(\frac{5}{2}),00\rangle$ states remain degenerate indicates that these centers are weakly (or not) coupled to the noncubic terms.

The energies of the $^4T_1$ electronic states are given in Fig. 11.

C. $^4T_2$ states

The vibronic structure of the $^4T_2$ states for the cubic centers consists of two lines separated by 4 cm^{-1} and one broad and weak line at high energy. Figure 7 shows that the structure of the SF_1 and SF_2 centers differs from that of the cubic centers only by the energy separation of the two lines at lower energy.

In order to interpret the vibronic structure of axial centers, we diagonalized $\mathcal{H}_{SO}+\mathcal{H}_{JT}$ by taking into account six phonons (168×168 matrix) and varying the Huang-Rhys parameter S from 0 to 2. Theoretical structures in agreement with those observed in axial sites were obtained by neglecting the second-order spin-orbit interaction and taking S in the range $0.4 \leq S \leq 0.8$ in order to account for the strong-intensity transfer which, as for the centers c, is observed in SF_1 and SF_2 centers. The vibronic shifts and structures are given in Fig. 12 and Table III (a good fitting with the observed fine-structure pattern is obtained with $S \sim 0.4$ for the centers SF_1 and $S \sim 0.5$ for the centers SF_2, the energy of the effective phonon being 100 cm^{-1}). (For the centers w we took $S = 0.6$.)

The electronic levels of the $^4T_2$ states are represented in Fig. 13.

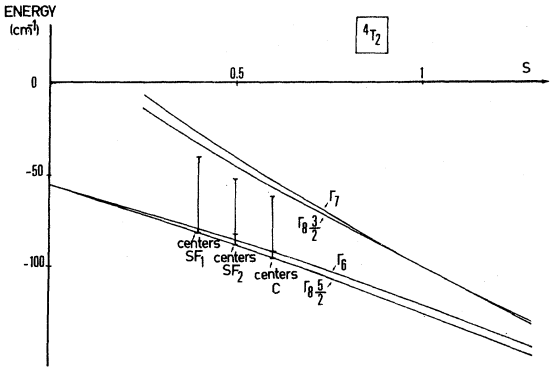

FIG. 12. Theoretical splittings and shifts of the fundamental vibronic lines of a $^4T_2$ state of Mn^{++} in the case of a Jahn-Teller coupling to E vibrational modes. $S = E_{JT}/\hbar\omega_E = 100$ cm^{-1}. The points correspond to the energy levels given in Fig. 7.

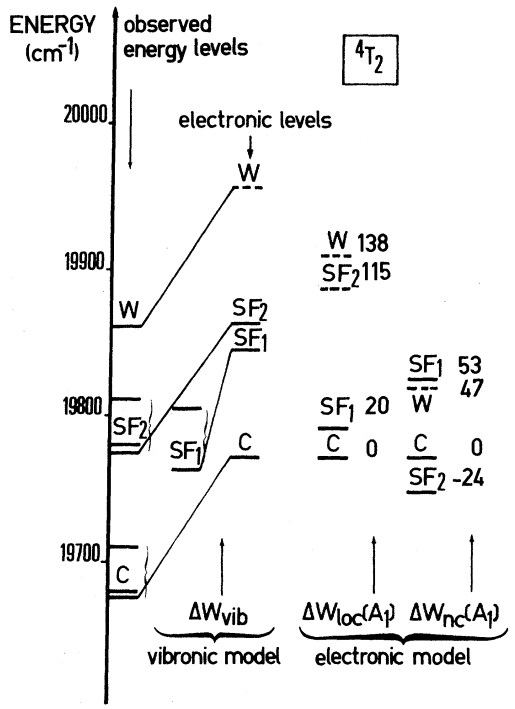

FIG. 13. Shifts (in cm^{-1}) of the $^4T_2$ states of the centers SF_1, SF_2, and w.

VI. DISCUSSION AND CONCLUSION

Coming back to an overall view of the fundamental vibronic states of the ^4E, $^4T_1$, and $^4T_2$ states of Mn^{++} in cubic and axial centers, several remarks and comments must be made.

First, all the observed fine-structure patterns have been interpreted in detail. Not only the relative positions of the fine-structure lines but also the relative dipole strengths of the lines are in excellent agreement with experiments.

Second, the vibronic shifts ΔW_{vib} have been deduced from an analysis of the fine-structure patterns, and the gravity centers of the electronic states ^4E, $^4T_1$, and $^4T_2$ for the cubic and axial centers have been obtained by simply adding ΔW_{vib} to the gravity centers of the observed energy levels. These electronic states are given in Figs. 9, 11, and 13 for the ^4E, $^4T_1$, and $^4T_2$ states, respectively.

Third, it is important to remark that having interpreted the fine-structure patterns in terms of the Jahn-Teller effect and determined the electronic states of the cubic and axial centers, the main purpose of this paper has been achieved.

Finally, for completeness, we will briefly examine the origin of the electronic interactions of A_1 sym-

TABLE III. $^4T_1$ states for the centers c, SF_1, SF_2, and w.

$^4T_1$	Energy of the FVL's (cm^{-1})	Nature of the FVL's	Huang-Rhys factor S	Vibronic shifts ΔW_{vib} (cm^{-1})[a]	$\Delta W_{loc}(A_1)$ cm^{-1}	$\Delta W_{nc}(A_1)$ (cm^{-1})
c (cubic centers)	17897	$\|\Gamma_7\rangle;\frac{3}{\sqrt{10}}\|\Gamma_8(\frac{3}{2})\rangle-\frac{1}{\sqrt{10}}\|\Gamma_8(\frac{5}{2})\rangle$				
	17887	$\|\Gamma_6\rangle;\frac{1}{\sqrt{10}}\|\Gamma_8(\frac{3}{2})\rangle+\frac{3}{\sqrt{10}}\|\Gamma_8(\frac{5}{2})\rangle$	1.9	190	0	0
SF_1 (stacking fault)	18017	$\|\Gamma_7\rangle;\frac{3}{\sqrt{10}}\|\Gamma_8(\frac{3}{2})\rangle-\frac{1}{\sqrt{10}}\|\Gamma_8(\frac{5}{2})\rangle$				
	18006	$\|\Gamma_6\rangle;\frac{1}{\sqrt{10}}\|\Gamma_8(\frac{3}{2})\rangle+\frac{3}{\sqrt{10}}\|\Gamma_8(\frac{5}{2})\rangle$	1.9	190	27	92
SF_2	17978	Γ_6				
	17980	$\Gamma_8(\frac{3}{2})$[b]				
	17987	Γ_7	~1.4	140	157	−115
	17991	$\Gamma_8(\frac{5}{2})$[b]				
w (wurtzite)	18102[c]		~1.9	~190	188	~22

[a]Vibronic shifts of the center of gravity of the fine-structure lines with respect to the $^4T_1$ electronic states.
[b]A splitting of these states is observed in uniaxial stress experiments for an applied pressure $\vec{P}$ parallel to the $[1\bar{1}0]$ axis.
[c]From Ref. 16.

metry which govern the shifts of the electronic states of the axial centers with respect to the electronic states of the cubic centers. This problem has already been considered in Sec. V in the case of the ^4E states. We have shown that the shifts of the ^4E states can be described in terms of slight dilatations of the MnS_4 clusters associated with the axial centers. (The dilatation of each cluster is given in the last column of Table I.) This description is in agreement with covalent models which predict that the ^4E states are sensitive to dilatations of the MnS_4 clusters[21,22] and with uniaxial stress experiments which show that these states are sensitive to strains $\epsilon(A_1)$.

This study of the ^4E states suggests that the perturbation of the cubic field $\Delta\mathcal{H}_c(A_1)$ associated with each axial center can be decomposed into a local perturbation $\Delta\mathcal{H}_{loc}(A_1)$ due to slight dilatations of the MnS_4 clusters and a nonlocal perturbation $\Delta\mathcal{H}_{nc}(A_1)$ due to the crystal field $[\Delta\mathcal{H}_c(A_1)]_V$; the ^4E states being primarily sensitive to $\Delta\mathcal{H}_{loc}(A_1)$ and the triplet states being sensitive to both $\Delta\mathcal{H}_{loc}(A_1)$ and $\Delta\mathcal{H}_{nc}(A_1)$. Therefore, for each axial center, the contribution of $\Delta\mathcal{H}_{loc}(A_1)$ to the ^4E, $^4T_1$, and $^4T_2$ states will be calculated from the dilatation of the MnS_4 clusters and the OLCC's to A_1 strains. Then, we will deduce the contribution of $\Delta\mathcal{H}_{nc}(A_1)$. It must be noted that no fitting parameter will be used in the following when we will separate the contributions of $\Delta\mathcal{H}_{loc}(A_1)$ and $\Delta\mathcal{H}_{nc}(A_1)$.

Following this procedure the shifts $\Delta W_{loc}(A_1)$ for the $^4T_1$ states are equal to 1.8 times the shifts $\Delta W_{loc}(A_1)$ of the ^4E states as deduced from the ratio of the OLCC's to A_1 strains in the $^4T_1$ and ^4E states. The shifts $\Delta W_{nc}(A_1)$ due to distant neighbors are simply obtained by subtracting those due to local strains from the overall electronic shifts (see Fig. 11 and Table III). For the $^4T_2$ states, the shifts attributed to local strains were obtained by comparing the OLCC's to A_1 strains in the $^4T_2$ states (18000 cm^{-1}/unit strain) and in the $^4T_1$ states (24500 cm^{-1}/unit strain) (see Fig. 13 and Table II).

It must be emphasized that the validity of the model can be checked by analyzing the consistency of the shifts associated with distant interactions A_1 in the LR approximation (this approximation is presented in Sec. V A). From the shifts $\Delta W_{nc}(A_1)$ obtained in the $^4T_1$ and $^4T_2$ states, we see that the LR approximation is in fact roughly satisfied for all centers.

Although further refinements of our treatment of electronic interactions are undoubtedly necessary, the chosen basic Hamiltonian and the method proposed to measure all relevant interactions give for the first time a unified description of several optical states of a d ion in a polymorph. A development of the rigid-ion model[23,24] for analyzing the local strains in the vicinity of a SF and in wurtzite as well as a detailed crystal-field model for distant interactions would be very helpful for building a complete physical model.

*Present address: Physics Department, University of Sétif, Sétif, Algeria.
†Equipe de Recherche associée au Centre National de la Recherche Scientifique.

[1]For reviews see, for example: M. D. Sturge, in *Solid State Physics*, edited by F. Seitz, D. Turnbull, and H. Ehrenreich (Academic, New York, 1967), Vol. 20; F. S. Ham, in *Electron Paramagnetic Resonance*, edited by S. Geschwind (Plenum, New York, 1972); R. Englman, *The Jahn-Teller Effect in Molecules and Crystals* (Wiley, New York, 1972).

[2]P. Edel, C. Hennies, Y. Merle d'Aubigné, R. Romestain, and Y. Twarowski, Phys. Rev. Lett. 28, 1268 (1972).

[3]A. M. Stoneham and M. Lanoo, J. Phys. Chem. Solids 30, 1769 (1969).

[4]F. S. Ham, Phys. Rev. Lett. 28, 1048 (1972).

[5]A. Hjortsberg, B. Nygren, J. T. Vallin, and F. S. Ham, Phys. Rev. Lett. 39, 19, 1233 (1977).

[6]W. L. Roth, in *Physics and Chemistry of II-VI Compounds*, edited by M. Aven and J. S. Prener (North-Holland, Amsterdam, 1967).

[7]G. A. Slack, F. S. Ham, and R. M. Schrenko, Phys. Rev. 152, 1, 376 (1966); F. S. Ham and G. A. Slack, Phys. Rev. B 4, 777 (1971).

[8]U. Kaufman, P. Koidl, and D. F. Schirmer, J. Phys. C 6, 310 (1973).

[9]A. I. Ryskin and G. I. Khil'ko, Opt. Spectrosc. 31, 405 (1971); Sov. Phys. Solid State 13, 153 (1971); A. I. Ryskin, L. G. Suslina, G. I. Khil'ko, and E. B. Shadrin, Phys. Status Solidi 49, 875 (1972).

[10]B. Clerjaud and A. Gélineau, Phys. Rev. A 9, 2832 (1974).

[11]J. T. Vallin, G. A. Slack, S. Roberts, and A. E. Hughes, Phys. Rev. B 2, 4313 (1970).

[12]R. Parrot, C. Naud, C. Porte, D. Fournier, A. C. Boccara, and J. C. Rivoal, Phys. Rev. 17, 3, 1057 (1978).

[13]R. Parrot, C. Naud, and F. Gendron, Phys. Rev. B 13, 9, 3748 (1976).

[14]C. Naud, C. Porte, F. Gendron, and R. Parrot, Phys. Rev. B 20, 3333 (1979).

[15]R. Parrot and C. Blanchard, Phys. Rev. B 6, 3992 (1972).

[16]B. Lambert, T. Buch, and A. Geoffroy, Phys. Rev. B 8, 863 (1973).

[17]W. Busse, H. E. Gumlich, A. Geoffroy, and R. Parrot, Phys. Status Solidi B 93, 591 (1979).

[18]F. S. Ham, Phys. Rev. 166, 307 (1968).

[19]This value is that of the low-frequency mode chosen by Ham and Slack in interpreting the optical spectra of Fe^{2+} in ZnS. [F. S. Ham and G. A. Slack, Phys. Rev. 4, 777 (1971).] It is also approximately that chosen by Vallin and Watkins in interpreting the EPR spectra of ZnS:Cr [J. T. Vallin and G. D. Watkins, Phys. Rev. B 9, 2051 (1974); see also C. S. Kelley and F. Williams, *ibid.* 2, 3 (1970).] Furthermore, such a relatively low value for the energy of the effective mode of E symmetry is needed in order to interpret the strong selective intensity transfer appearing in the $^4T_2$ states.

[20]W. Busse, H. E. Gumlich, B. Meissner, and D. Theis, J. Lumin. 12/13, 693 (1976).

[21]C. Blanchard and R. Parrot, Solid State Commun. 10, 413 (1972).

[22]L. L. Lohr, Jr., J. Chem. Phys. 45, 3611 (1966).

[23]M. Vandevyver and P. Plumelle, Phys. Rev. 17, 675 (1978).

[24]K. Kunc, Ann. Phys. (Paris) No. 8, 319, Masson (1973–1974); Phys. Status Solidi 72, 229, 249 (1975).